The Local Structure of Molten CdBr$_2$

Hideaki Shiwaku[a], Yoshihiro Okamoto[a,b], Tsuyashi Yaita[a,b], Shinichi Suzuki[b], Kazuo Minato[b], and Hajime Tanida[c]

[a] Synchrotron Radiation Research Center, Japan Atomic Energy Research Institute, Kouto, Mikazuki-cho, Sayo-gun, Hyogo-ken 679-5148, Japan
[b] Department of Materials Science, Japan Atomic Energy Research Institute, Tokai-mura, Naka-gun, Ibaraki 319-1195, Japan
[c] Japan Synchrotron Radiation Research Institute, Kouto, Mikazuki-cho, Sayo-gun, Hyogo-ken 679-5198, Japan

Reprint requests to Dr. H. S.; Fax: +81-791-58-2740; E-mail: shiwaku@spring8.or.jp

The local structure of molten CdBr$_2$ was investigated by high temperature X-ray absorption fine structure (XAFS) analysis. The quartz cell designed for hygroscopic high temperature molten salts was successfully used in the measurement. At room temperature the nearest neighbor Cd^{2+}-Br$^-$ distance decreased from 2.71 Å in solid state to 2.60 Å in the molten state. The coordination number decreased from 6 to 4 on melting. The obtained structural parameters showed that (CdBr$_4$)$^{2-}$ is predominant in molten CdBr$_2$.

Key words: XAFS; Molten Salt; Structure; Synchrotron Radiation.

1. Introduction

We have developed a technique to measure the high temperature X-ray absorption fine structure (XAFS) of molten salts [1] and measured some halide melts [2, 3]. The XAFS technique is very useful to study the behavior of polyvalent metal ions in salt baths like the LiCl-KCl eutectic mixture. For example, the concentration of UCl$_3$ in LiCl-KCl is usually smaller than 1% in the pyrochemical reprocessing of spent nuclear fuels [4]. The XAFS method is unique in obtaining information on the local structure around the metal ion in such a dilute solution. In addition, using high energy X-rays is an effective way to extend molten salt XAFS measurements. In the present work, the local structure of molten CdBr$_2$ was investigated by using molten salt XAFS analysis.

2. Experimental

The XAFS spectra were measured at the BL11XU beamline in SPring-8 (Harima, Japan). The operating energy and the ring current were 8 GeV and 99 mA (top-up mode [5]), respectively. The radiation monochromatized by double Si(111) crystals with liquid nitrogen cooling [6, 7] was used. In the measurement, an insertion device (ID) was adjusted to obtain the strongest beam intensity for each energy point.
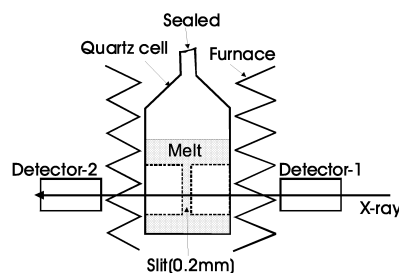

Fig. 1. Scheme of the high temperature molten salt XAFS measurement.

Thus, a continuous X-ray beam for a wide energetic range was available in the XAFS measurement in spite of the beamline with undulator.

The measurement system used in the present work is shown in Figure 1. A quartz tube having a narrow slit (0.2 mm width) was designed for molten salt XAFS measurements. The solid CdBr$_2$ sample (99.9% purity), loaded in the quartz cell, was dried at 573 K under reduced pressure for 1 day. After that, the cell was sealed off under reduced pressure as shown in the Figure 1. The slit part was filled with the melt above the melting point of CdBr$_2$ (839 K). The melt at the slit part has 0.2 mm thickness automatically. XAFS spectra were obtained based on the Cd K-edge ($E_0 =$ 26.711 keV). The measurements were performed in an energy range 26.2 to 28.2 keV at 900 K. Stepped scan
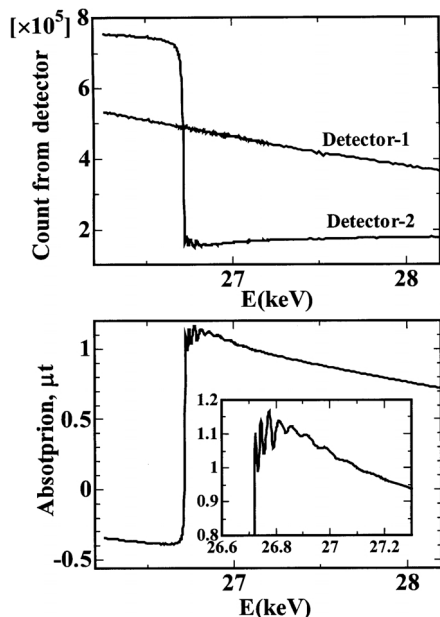
Fig. 2. Intensity data from the detector-1 and -2 and raw XAFS spectrum of solid Cd foil based on the Cd K-absorption edge ($E_0 = 26.711$ keV).

measurements for 1 s were performed to obtain the X-ray absorption spectra.

The computer program code WinXAS ver. 2.3, developed by Ressler [8], and the XAFS simulation code FEFF8 [9] were used in the XAFS data analysis. A phase shift and backscattering amplitude parameters to be used in the curve fitting of the WinXAS were simulated by using the FEFF8. Coordination number N_j, interionic distance r_j and Debye-Waller factor σ_j^2 were obtained from the curve fitting in k-space. In the present work, the cumulant expansion technique [10] was used to treat an anharmonic vibration effect. Thus, the following equation was used in the fitting procedure:

$$\chi(k) =$$
$$\sum_j N_j S_j(k) F_j(k) \exp(-2\sigma_j^2 k^2) \exp(-r_j/\lambda)$$
$$\cdot \exp(\frac{2}{3}C4_j k^4) \sin(2kr_j + \phi_j(k) - \frac{4}{3}C3_j k^3)/(kr_j^2),$$

where N_j = coordination number (CN) of ion j around central ion i, $S_j(k)$ = amplitude reduction factor mainly due to many-body effect, $F_j(k)$ = backscattering amplitude for each neighboring atom, σ_j = Debye-Waller factor corresponding to thermal vibration, λ = electron mean free path, $\phi_{ij}(k)$ = total phase shift experienced
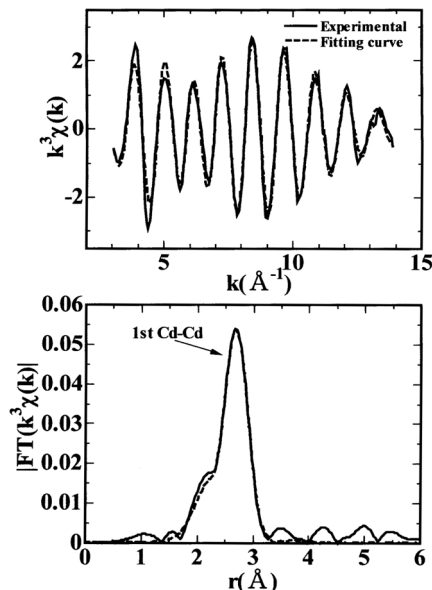

Fig. 3. XAFS function $k^3\chi(k)$ and Fourier transform $|FT(k^3\chi(k))|$ of solid Cd foil.

by a photoelectron, r_j = average distance of ion j from the central ion i, $C3, C4$ = 3rd and 4th cumulants.

3. Results and Discussions

3.1. Cd Metal Foil

At first, a Cd metal foil was used as a standard material, since we had to check the XAFS measurement system in an undulator beamline with the monochromator cooled by liquid nitrogen circulation [6]. The obtained X-ray count from the detectors and the XAFS spectrum of Cd foil are shown in Figure 2. No displacement due to the undulator and the liquid nitrogen circulation was found in the incident beam intensity. The incident X-ray beam was so stable that good quality XAFS data were obtained. The XAFS function $k^3\chi(k)$ and the Fourier transform function $|FT(k^3\chi(k))|$ are shown in Fig. 3, together with the curve fitting results. The experimental curve was nicely fitted by using the literature values [11]. Thus we concluded that the XAFS measurement of Cd K-edge in the beamline BL11XU is performed without any problems.

3.2. Solid and Molten CdBr₂

Raw XAFS curves of solid CdBr₂ at room temperature and molten CdBr₂ at 900 K are shown in Fig-
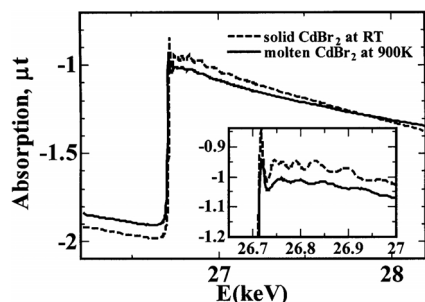
Fig. 4. Raw XAFS spectra of solid CdBr$_2$ at room temperature (RT) and molten CdBr$_2$ at 900 K.
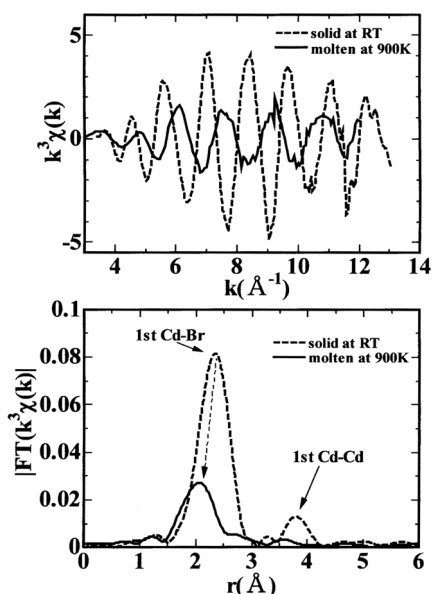

Fig. 5. XAFS function $k^3\chi(k)$ and Fourier transform $|\mathrm{FT}(k^3\chi(k))|$ of solid and molten CdBr$_2$.

ure 4. Good quality data, similar to the solid Cd foil, were obtained for CdBr$_2$ in the high temperature liquid state. The XAFS function $k^3\chi(k)$ and Fourier transform function $|\mathrm{FT}(k^3\chi(k))|$ of solid and molten CdBr$_2$ are shown in Figure 5. The 1st peak in the $|\mathrm{FT}(k^3\chi(k))|$ function is assigned to the 1st Cd^{2+}-Br$^-$ correlation. The 2nd peak, corresponding to the 1st Cd^{2+}-Cd^{2+} correlation, is found in the solid state. On the other hand, a very weak peak is found around 3.6 Å in the $|\mathrm{FT}(k^3\chi(k))|$ function of molten CdBr$_2$. The oscillation of signal in the $k^3\chi(k)$ function and the 1st peak in the $|\mathrm{FT}(k^3\chi(k))|$ function decrease on melting. In addition, the phase of the signal in the $k^3\chi(k)$ function shifts to higher k after melting. This shows that the local structure of CdBr$_2$ changes on melting.
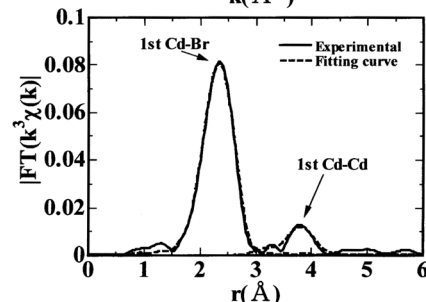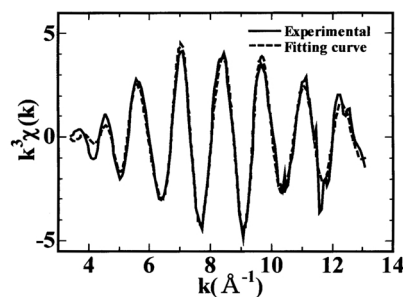

Fig. 6. Curve fitting results of the XAFS function $k^3\chi(k)$ and magnitude of the Fourier transform $|\mathrm{FT}(k^3\chi(k))|$ of solid CdBr$_2$ at room temperature.
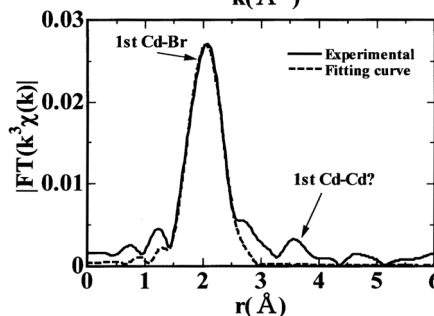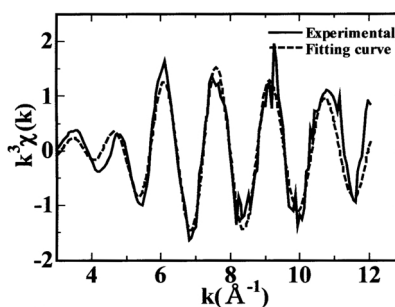

Fig. 7. Curve fitting results of the XAFS function $k^3\chi(k)$ and magnitude of the Fourier transform $|\mathrm{FT}(k^3\chi(k))|$ of molten CdBr$_2$ at 900 K.

Curve fitting results are shown in Figs. 6 and 7. The structural parameters from the curve fitting analysis are listed in Table 1. The distance and coordination number of the 1st Cd^{2+}-Br$^-$ correlation of the

Table 1. Structural parameters of solid and molten CdBr$_2$ from Cd K-edge XAFS.

	$S_j(k)$	N_j	r_{ij} (Å)	σ_j^2 (Å^2)	$C3$ (10^3 Å^3)	$C4$ (10^{4}Å^4)	residual
Solid CdBr$_2$							
Cd^{2+}-Br$^-$	0.816	5.8	2.71	0.0093	–	–	14.3
Cd^{2+}-Cd^{2+}		5.9	3.95	0.0150	–	–	
Molten CdBr$_2$							
Cd^{2+}-Br$^-$	0.745	4.1	2.60	0.0185	1.456	1.560	2.6
Cd^{2+}-Cd^{2+}*		(3.9)	(3.81)	(0.0414)	(1.328)	(6.940)	

* The 1st Cd^{2+}-Cd^{2+} correlation of molten CdBr$_2$ did not give clear convergence.

solid at room temperature is 2.71 Å and 5.8, respectively. It is almost the same as the data in [12]. These values decrease to 2.60 Å and 4.1 on melting, suggesting that the 4-fold (CdCl$_4$)$^{2-}$ coordination structure is predominant in molten CdBr$_2$. The drastic phase change in the $k^3\chi(k)$ function is assigned to the decreasing Cd^{2+}-Br$^-$ distance on melting. This result is very close to melting behavior of CdCl$_2$ [13 – 15]. The 1st Cd^{2+}-Cd^{2+} correlation also shows similar behavior. The distance and coordination number decrease on melting.

4. Conclusion

A high-temperature XAFS measurement system, using a specially designed quartz cell, was developed in the present work. We confirmed from the curve fitting analysis that the local structure of molten CdBr$_2$ changes from the 6-fold to the 4-fold coordination on melting.

[1] Y. Okamoto, M. Akabori, H. Motohashi, A. Itoh, and T. Ogawa, Nucl. Instr. Meth. Phys. Res. A **487**, 605 (2002).

[2] Y. Okamoto, M. Akabori, H. Motohashi, H. Shiwaku, and T. Ogawa, J. Synchrotron Rad. **8**, 1191 (2001).

[3] Y. Okamoto, H. Shiwaku, T. Yaita, H. Narita, and H. Tanida, J. Mol. Struct. **641**, 71 (2002).

[4] O. Shirai, T. Iwai, Y. Suzuki, Y. Sakamura, and H. Tanaka, J. Alloys & Comp. **271 – 273**, 685 (1998).

[5] H. Tanaka, T. Aoki, T. Asaka, S. Date, K. Fukami, Y. Furukawa, H. Hanaki, N. Hosoda, T. Kobayashi, N. Kumagi, M. Masaki, T. Masuda, S. Matsui, A. Mizuno, T. Nakamura, T. Nakatani, T. Noda, T. Ohata, H. Ohkuma, T. Ohshima, M. Oishi, S. Sasaki, J. Schimizu, M. Shoji, K. Soutome, M. Suzuki, S. Suzuki, S. Takono, M. Takoa, T. Takashima, H. Takebe, K. Tamura, R. Tanaka, T. Taniuchi, Y. Taniuchi, K. Tsumaki, A. Yamashita, K. Yanagida, H. Yonehara, T. Yorita, M. Adachi, K. Kobayashi, and M. Yoshida, Top-up Operation at SPring-8 – Towards Maximizing the Potential of a 3rd Generation Light Source, Proceedings of the 9th European Particle Accelerator Conference, 5 to 9 July, 2004, Lucerne.

[6] H. Shiwaku, T. Mitsui, K. Tozawa, K. Kiriyama, T. Harami, and T. Mochizuki, AIP Conference Proceedings **705**, 659 (2004).

[7] K. Tozawa, K. Kiriyama, T. Mitsui, H. Shiwaku, and T. Harami, AIP Conference Proceedings **705**, 671 (2004).

[8] T. Ressler, J. Synchrotron Rad. **5**, 118 (1998).

[9] A. L. Ankudinov and J. J. Rehr, Phys. Rev. B**56**, R1712 (1997).

[10] G. Bunker, Nucl. Instrum. Methods Phys. Res. **207**, 437 (1983).

[11] R. W. G. Wyckoff, Crystal Structures, vol. 1, p. 11, John Wiley & Sons, New York 1963.

[12] R. W. G. Wyckoff, Crystal Structures, vol. 1, p. 276, John Wiley & Sons, New York 1963.

[13] Y. Takagi, N. Itoh, and T. Nakamura, J. Chem. Soc., Faraday Trans. I, **85**, 493 (1989).

[14] B. Børresen, G. A. Voyiatzis, and G. N. Papatheodorou, Phys. Chem. Chem. Phys. **1**, 3309 (1999).

[15] Y. Okamoto, H. Shiwaku, T. Yaita, S. Suzuki, K. Minato, and H. Tanida, Z. Naturforsch. **59a**, 819 (2004).